Original Article | Journal of Biosystems Engineering

J. of Biosystems Eng. 40(4):417-427. (2015. 12)
http://dx.doi.org/10.5307/JBE.2015.40.4.417

eISSN : 2234-1862
pISSN : 1738-1266

Band Selection Using Forward Feature Selection Algorithm for Citrus Huanglongbing Disease Detection

Anurag R. Katti[1], W. S. Lee[2]*, R. Ehsani[3], C. Yang[4]

[1]*Electrical and Computer Engineering, University of Florida, Gainesville, Florida 32611, USA*
[2]*Agricultural and Biological Engineering, University of Florida, Gainesville, Florida 32611, USA*
[3]*Agricultural and Biological Engineering, Citrus Research and Education Center, University of Florida, Lake Alfred, Florida 33850, USA*
[4]*USDA-ARS Southern Plains Agricultural Research Center, Areawide Pest Management Research Unit, 2771 F and B Road, College Station, Texas 77845, USA*

Received: September 21st, 2015; Revised: October 22nd, 2015; Accepted: November 5th, 2015

Abstract

Purpose: This study investigated different band selection methods to classify spectrally similar data - obtained from aerial images of healthy citrus canopies and citrus greening disease (Huanglongbing or HLB) infected canopies - using small differences without unmixing endmember components and therefore without the need for an endmember library. However, large number of hyperspectral bands has high redundancy which had to be reduced through band selection. The objective, therefore, was to first select the best set of bands and then detect citrus Huanglongbing infected canopies using these bands in aerial hyperspectral images. **Methods:** The forward feature selection algorithm (FFSA) was chosen for band selection. The selected bands were used for identifying HLB infected pixels using various classifiers such as K nearest neighbor (KNN), support vector machine (SVM), naïve Bayesian classifier (NBC), and generalized local discriminant bases (LDB). All bands were also utilized to compare results. **Results:** It was determined that a few well-chosen bands yielded much better results than when all bands were chosen, and brought the classification results on par with standard hyperspectral classification techniques such as spectral angle mapper (SAM) and mixture tuned matched filtering (MTMF). Median detection accuracies ranged from 66-80%, which showed great potential toward rapid detection of the disease. **Conclusions:** Among the methods investigated, a support vector machine classifier combined with the forward feature selection algorithm yielded the best results.

Keywords: Bayesian classification, Hyperspectral, K nearest neighbor, Multi-modal Bayesian classification, Support vector machine

Introduction

Huanglongbing (HLB) or citrus greening disease (Figure 1) is believed to have spread from China. The main carriers of the disease are two psyllids of which the Asian citrus psyllid (*Diaphorina citri*) is the most common in Florida, USA. The bacterium causing the disease is *Candidatus Liberibacter asiaticus* (Garnier et al., 2000). There are many strains of the bacterium that have been observed across Asia, Africa, Brazil, etc. (Brlansky et al., 2005).

The disease affects the vascular system of the plant and affects the growth of the plant, leaves and fruit. The characteristic symptom is blotchiness of leaves and yellowing of the veins in the leaves. The fruits also develop a yellow color, uneven ripening and tend to be asymmetric. The tree once infected dies in 3-5 years. Currently there is no cure for this disease. As of November, 2011, 37 counties with over 4,012 square mile sections (Albritton, 2012) had been infected in Florida alone. The citrus industry is

***Corresponding author:** W. S. Lee
Tel: +1-352-392-1864 Ext. 207; **Fax:** +1-352-392-4092
E-mail: wslee@ufl.edu

Figure 1. HLB infected fruits and leaves from an orange grove in the Citrus Research and Education Centre, Lake Alfred, Florida: (a) infected fruit, and (b) three infected leaf samples at different stages of infection and a healthy leaf sample.

worth $9 billion (USDA, 2012) to the state of Florida with nearly 243,000 ha of land dedicated to citrus production, making HLB a big concern.

The most reliable method to test if a tree has been infected is the polymerase chain reaction (PCR) method, but it is expensive, time consuming and labor intensive. Visual monitoring can be used at an advanced stage when symptoms begin to show on the leaf and fruit. But even then it is possible to conflate the symptoms with other less threatening conditions which show similar symptoms, for example, zinc deficiency which causes yellowing of leaves. It would be useful if the disease can be detected accurately before the infection becomes severe and visual symptoms arise.

Aerial hyperspectral imagery has made it easy to view large tracts of land at once, and the increased spectral resolution allows for the detection and classification of features based on spectral signatures. Previous attempts at hyperspectral image classification have been successful in detecting citrus canker (Qin et al., 2009), bacterial leaf blight (Yang, 2010), and diseases in lettuce plants (Matsuo et al., 2006), to name a few. Some of the most commonly used classification methods are support vector machines (SVM) (Candade and Dixon, 2004; Demir and Erturk, 2007), artificial neural networks (ANN) (Kuo et al., 2008; Candade and Dixon, 2004), Gaussian classifier (Kuo et al., 2008), and K-nearest neighbor (KNN) (Kuo et al., 2008; Yang, 2010).

Vegetation indices - metrics calculated using data from selected bands are also extremely popular classification techniques. Different indices have been used to detect ganoderma basal stem rot disease in oil palms (Shafri and Hamdan, 2009), rice sheath blight disease (Qin and Zhang, 2005) and yellow rust infection in wheat (Huang et al., 2007). Normalized difference vegetation index (NDVI) (Rouse et al., 1973) is probably one of the most popular vegetative indices and has been also employed in this study to detect vegetation from background.

Beside vegetation indices, another method to overcome the large number of hyperspectral bands - usually running into the hundreds - is dimensionality or band reduction. These high resolution bands are spectrally very close and therefore adjacent bands tend to have a high degree of correlation. Principal component analysis (PCA) (Bajwa et al., 2004) and minimum noise fraction (MNF) (Boardman and Kruse, 1994) are commonly used at a pre-processing stage. One or both of these methods were used by Kumar et al. (2012) and Li et al. (2012) for citrus HLB detection. Mixture tuned matched filtering (MTMF), linear spectral unmixing (LSU), spectral angle mapper (SAM) and other commonly used hyperspectral image analysis techniques were explored in the same studies. Partial least squares discriminant analysis (PLS-DA) is one of the commonly used methods. Williams et al. (2012) implemented PLS-DA to discriminate different species and strains of fungi associated with maize from hyperspectral images in 1000-2500 nm, and reported 60-80% correct prediction accuracies. Kong et al. (2013) applied PLS-DA method to

identify rice seed cultivars from hyperspectral images of rice seeds in 870-1730 nm, and achieved 80-100% classification accuracies depending on different models. Some more popularly used classification methods have been surveyed by Sankaran et al. (2010).

However, the low spatial resolution when compared to the size of the plant or tree causes each tree to be represented by only a few pixels. Therefore, each pixel is a mixture of both healthy and infected regions making classification more difficult. While many techniques that unmix these components exist, in this study we attempted to classify without unmixing these similar spectra, and the results were compared with the unmixed results by Li et al. (2012).

Thus the overall goal of this study was two-fold:

1. Reduce the dimensionality of hyperspectral data by picking the most appropriate bands using the forward feature selection algorithm (FFSA) (Whitney, 1971)
2. Classify spectrally similar data on the basis of small spectral differences using the bands selected by FFSA.

The FFSA method is explained in the method section. Two hyperspectral (HS) images were used to test the algorithms - an image taken in 2010 whose classes (healthy and infected) were very similar, and an image from 2011 with better spatial resolution and hence slightly better separation between the classes.

Materials and Methods

Materials

In 2010, hyperspectral images were acquired at the Southern Garden (SG) grove in Hendry County, Florida, USA using the airborne imaging systems described by Yang et al. (2003) and Yang (2010). The images were acquired on a clear day from an altitude of about 1,500 m at 2:30 pm on December 3, 2010. The image contained 128 bands between 457.2 - 921.7 nm with an interval of 3.6 nm between bands and a spatial resolution of 1 m. The orange variety was Valencia.

The SG grove data had three classes: healthy (HLTY), HLB symptomatic (HLBS), and PCR positive for HLB but showing no symptoms (HLBNS), all confirmed with PCR testing of the leaves. The HLTY samples were collected from trees showing no HLB symptoms, while the HLBS samples were taken from trees which showed more severe symptoms. The non-symptomatic samples were infected but showed no visible symptoms. These were used for calibration and validation but not for training. The HLTY and HLBS samples were used in all stages of learning and classification as shown in Table 1.

The 2011 image was acquired on December 14 at the Citrus Research and Education Center (CREC) citrus grove in Lake Alfred, Florida, USA at noon on a clear day from an altitude of 640 m. An airborne hyperspectral camera unit - AISA EAGLE VNIR hyper spectral imaging sensor (400 - 1000 nm spectral range with a total of 128 spectral bands and a spectral resolution of approximately 5 nm) was used for imaging. The images had a spatial resolution of 0.5 m. Of the 128 bands, the first 10 and last 20 bands (up to 440 nm and beyond 900 nm) were noisy and removed from the dataset. The orange variety was Hamlin.

The 2011 data had only two kinds of samples: healthy (HLTY) and infected (HLB). The infected trees were confirmed with PCR testing; the healthy trees were only confirmed by visual inspection by a ground-truthing expert at the CREC. Figure 2 shows a 2011 color infrared image of the CREC grove.

Both the 2010 and 2011 HS images were converted to reflectance images using tarps of different grey levels. Their reflectance was measured using a handheld spectrometer (HR-1024, Spectra Vista Corporation, Poughkeepsie, NY, USA) and matched with the aerial images. Five 3 m × 3 m tarps with grey levels of 3%, 10%, 30%, 45%, and

Table 1. Summary of 2010 and 2011 hyperspectral image data: HLTY = healthy, HLB = infected, HLBS = infected and symptomatic, and HLBNS = infected with no symptoms

Image	Pixel samples (pixels)	Training set (pixels)	Calibration set (pixels)	Validation set (pixels)
2010 SG image	52 HLTY 109 HLBS 16 HLBNS	62 (22 HLTY + 40 HLBS)	60 (15 HLTY + 35 HLBS + 10 HLBNS)	55 (15 HLTY + 34 HLBS + 6 HLBNS)
2011 CREC image	90 HLTY 154 HLB	80 (30 HLTY + 50 HLB)	80 (30 HLTY + 50 HLB)	84 (30 HLTY + 54 HLB)

Figure 2. Hyperspectral image of a block in the CREC grove acquired in 2011.

60% were used for the 2010 image but only one white tarp with an average reflectance of 56% was used for the 2011 image. The empirical line method was used to convert the raw digital number (DN) values to reflectance.

Both of the images were geo-referenced to UTM N17 projection with the datum WGS-84 using coordinates collected with an RTK GPS receiver (HiPer XT, Topcon, Livermore, CA, USA) with positioning error less than 15 mm. These coordinates were used with the images to determine the location of the infected and healthy plants in the images. The spectral data was divided into three datasets almost equally as shown in Table 1.

Methods

In this study, simple yet efficient algorithms were used for classification of citrus canopies. A method to improve the accuracy using band selection (using FFSA) was used in conjunction with these algorithms. The techniques used were KNN, naïve Bayes classifier (NBC), SVM and generalized local discriminant bases (LDB) technique. Simulations were carried out using Matlab (Mathworks, Natick, Massachusetts, U.S.A.).

To reduce execution time, only the pixels corresponding to ground truth points were used. These ground truth pixels were divided randomly into three groups - training, calibration and validation. Training data was used to generate a model from the dataset and the calibration was used to select the best model for optimum results. Multiple models can be generated using different sets of bands; calibration is therefore the process of selecting the band(s) which yield the best accuracy. The band(s) identified during calibration were used in the validation set to check the accuracy of the classifier.

However, even before training and calibration, the pixel data can be subjected to the processes of normalization or spectral difference - the analog of differentiation for discrete data. These were done to try and improve the separation between the classes, since the data of the two classes (HLTY and HLBS) appeared very similar, particularly the SG data set.

Since the training, calibration and validation groups were formed randomly, repeatability of the algorithm and consistency of results needed to be verified. Hence, the entire procedure was repeated multiple times with new training, calibration and validation sets generated randomly each time (referred to as a "run"). The different methods were compared based on the median of validation set classification accuracy over 100 runs. The median accuracy was chosen because it indicates a 50% chance of getting a better result. Described in the remaining sections are the various processing steps and the classification algorithms.

Normalization and difference spectra

Since the two classes appear very similar, different processes were tried to improve separation such as normalization and difference (first difference) operations. One of the simplest ways to normalize data is to convert all of them to the same range [0, 1]. This procedure can be used to correct for scaling and shifting of waveforms and highlight some features not apparent otherwise. Normalized spectrum (y) is calculated as:

$$y = (x - \min\{x\})/(\max\{x\} - \min\{x\}) \quad (1)$$

where x is the original spectrum.

Similarly, first difference of a signal is calculated as

$$x_i = (y_{i+1} - y_i) \quad (2)$$

where y_i is the reflectance in the i^{th} band and x_i is the first difference at the i^{th} band.

First difference of a signal can be used to compare the variation of signals across the wavelength spectrum. First difference highlights the difference between adjacent bands; if the relation between adjacent bands is different for the two classes, this method may improve the separation between them. For example, in case of citrus plants, it is known that HLB infected pixels are brighter while the

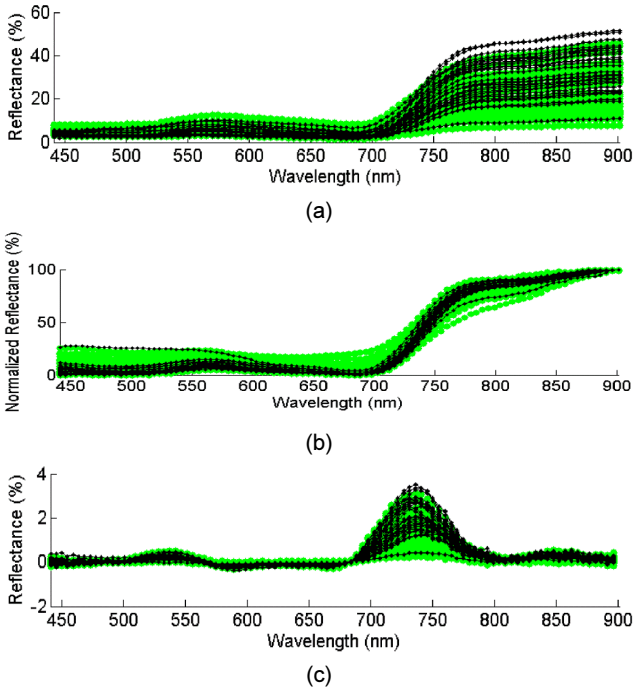

Figure 3. Comparison of original, normalized and 1st difference of spectra. HLB is displayed in green, and healthy in black: (a) original spectra, (b) normalized spectra, and (c) 1st difference of the original spectra.

healthy pixels are darker, so the relationship between adjacent bands in healthy pixels is not the same as in infected pixels.

Figure 3 shows the spectra of an unprocessed set of healthy and infected pixels, normalized and first difference spectra. For this case, better separation was observed between HLB (green) and healthy (black) spectra in the 450-550 nm and 650-700 nm range on normalization. For the first difference spectra, there is great difference between HLB and healthy spectra around 740 nm. While perfect classification may still not be possible even with processing due to the similarity of these classes, an improvement was observed.

With normalization and difference operations, three different types of processing of spectra, i.e., no processing, normalization and first difference can be performed on the data. Each of the three processing steps was combined with the classification methods described below.

Forward feature selection algorithm(FFSA)

Forward feature selection algorithm (FFSA) as described by Whitney (1971) was used to determine the subset of bands that would give the best classification results. The procedure is: for the chosen classification algorithm the single band with the highest accuracy is chosen. A new band is added to the previously selected band(s) iteratively to maximize classification accuracy. This procedure is repeated until all bands have been selected or the classification accuracy does not improve significantly (0% increase was the cutoff used in this study).

KNN classification

K nearest neighbor (KNN) classification method (Cover and Hart, 1967) is a supervised technique where the unknown data is classified to a group based on the class of its closest neighbor(s) from the training set. The factor 'K' denotes the number of neighbors to consider for classification purposes. When K=1, only the closest neighbor is considered and its class is assigned to the new sample. Two variations of KNN were implemented in this study - KNN1 and KNN2. KNN1 used only a subset of bands selected using FFSA, whereas in KNN2 all the bands were utilized.

SVM classification

Support vector machines (Melgani and Bruzzone, 2004) transform the training set to a higher dimension to improve separation between the classes. This method is very useful for data that cannot be linearly separated. By projecting to a higher dimension, differences between classes can be enhanced allowing linear classifiers. The vectors which indicate the least separation between the classes are called support vectors and training involves finding a transform that maximizes the distance between support vectors. Two variants of this algorithm, SVM1 and SVM2, were used. SVM1 used FFSA and SVM2 did not.

Naïve bayesian classification (NBC)

Naïve Bayesian classifier (NBC) (Cestnik, 1990) is a probabilistic approach to the classification problem. From the training data set, it develops a Bayesian probability distribution model for all the classes and classifies new data based on the model. The class with the highest likelihood of occurrence for a given sample is assigned to it. NBC also used FFSA (NBC1) and non-FFSA variant (NBC2).

Generalized local discriminant bases classification (LDB)

The top down generalized local discriminant bases approach of Kumar et al. (2001) identifies sets of adjacent

bands that generate a good classification result. Taking advantage of the high covariance between adjacent bands, the algorithm combines adjacent bands using some metric - mean, for example. In the top-down approach, the set of available bands is split into two smaller sets of adjacent bands. These are then further split into two smaller sets and so on until each set only has one band. Sets with more than one band are combined using the mean operator to form "group-bands". FFSA is applied on these group bands to select the ones which give the best accuracy.

In this study, group bands were generated in a bottom up manner instead of the top-down because it was observed that the accuracy was higher for a smaller number of bands than for a larger set, therefore combining smaller sets of bands was preferred to splitting larger sets into smaller ones. Despite using a bottom up approach, the algorithm is different from the bottom up approach of Kumar et al. (2001).

Results and Discussion

Results

For all the techniques, classification was allowed to progress from the learning stage only if the learning and calibration stages were able to achieve a calibration accuracy of at least 50% for both healthy and infected classes individually. This criterion was to ensure that the classifier is actually separating the two classes and not labelling all samples to one class. The condition also automatically ensured that overall training accuracy was at least 50%.

Comparison of performances was made based on the median classification accuracy of the validation stage. It must be noted that since the median is calculated separately for total, HLTY and HLB accuracies, the sum of HLTY and HLB pixels need not match the number of validation pixels. Another point of comparison was the accuracy of detecting HLB and HLTY pixels individually. A higher HLTY detection accuracy indicates a lower false positive rate (defined as the number of healthy pixels classified as infected and calculated as 100 - HLTY accuracy) which is a desired trait in a classifier. Due to the similarity of the two classes (particularly in the 2010 image), this was not entirely possible and the accuracy with which healthy pixels were detected was less than HLB in general, despite the roughly 70% overall accuracy. This was mainly due to the fewer number of HLTY samples, particularly for the SG data set which had very few HLTY pixels.

The 2010 data set showed poorer results in general because at the time of imaging the sun was not directly overhead but at an angle, and the spatial resolution of the image was also lower hence each pixel covered a larger area, increasing the chances of a pixel covering both

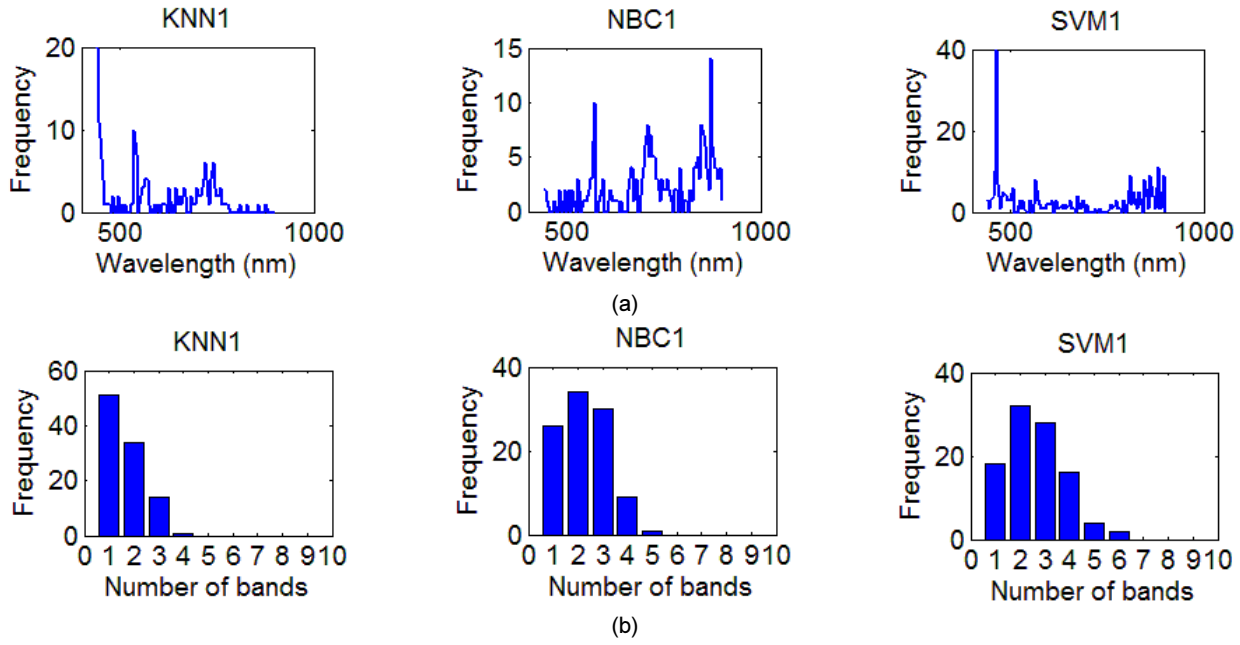

Figure 4. Histogram of the wavelengths selected and number of bands by the different FFSA incorporating techniques for CREC image classification: (a) histogram of frequency of wavelengths chosen, and (b) histogram of number of bands.

healthy and infected areas of a canopy. The 2011 CREC data set was slightly better because imaging was done at noon, and the spatial resolution was also better although still not as good as indoor measurements of Li et al. (2012).

The first objective of the study was band selection to reduce the number of bands from 128 (SG) or 98 (CREC). Figure 4 shows histogram plots of number of bands selected by each algorithm (based on FFSA) for the CREC grove image. It can be seen that less than 5 bands were chosen most time – a reduction of over 90%. This fulfils the first aim of the study. For the CREC image, the typical number of bands employed ranged between two and three with bands in the infrared range (>750 nm) selected most often. Other common, but less frequently selected bands located near the red edge (about 700 nm) and the green regions of the spectrum (>500 nm). While the median number of bands selected by other methods was between 2 and 3, KNN chose only 1 band.

The results for the SG grove image were also quite similar - the median number of bands selected was 2-3 with 6 being the highest (NBC1 and KNN1). The wavelengths between 600 and 800 nm were most often used by each of the methods for classification (Table 2). However, their frequencies were not as high as the CREC image and neither were the range of frequencies. Due to the similarity of the two classes, 50% individual class accuracy could not be achieved by any of the methods during most runs, therefore none of the bands selected in those runs are listed. This reduced the range and frequency of the bands.

Table 3 lists the results of classification using all the algorithms for the SG grove and it can be seen from the last column that in all but two cases, the data was either normalized or first difference was used. Clearly processed data was better at detecting infected pixels for the SG data set. There were also a lot of "disqualified results" which constituted results where the calibration accuracy did not exceed 50% for both healthy and infected. The number

Table 2. List of most frequently chosen bands for CREC and SG images

Image	Frequency	Method	Wavelengths (nm)
CREC (2011)	5	NBC1	555.8, 659.9, 669.4, 678.9, 693.1, 697.9, 707.4, 712.1, 716.9, 832.9, 842.6, 847.4, 852.3
		KNN1	477.6, 486.8, 491.3, 495.9, 500.5, 505.1, 509.7, 518.8, 570.0, 598.4, 617.3, 650.4, 740.6, 745.3, 754.9, 759.8, 764.7, 774.4
		SVM1	440.9, 477.6, 486.8, 491.3, 509.7, 570.0, 693.1, 702.6, 712.1, 716.9, 754.9, 759.8, 764.7, 769.5, 774.4, 784.2, 793.9, 818.3, 852.3, 862.0
	15	NBC1	None
		KNN1	754.9
		SVM1	570.0, 754.9, 759.8, 774.4
SG (2010)	5	NBC1	None
		KNN1	466.3, 524.3, 557.0, 604.2, 909.0
		SVM1	488.0, 593.3, 600.5, 658.6, 662.2, 763.8, 782.0, 792.9
	15	NBC1	None
		KNN1	None
		SVM1	763.8, 792.9

Table 3. Accuracy of all the algorithms for the SG grove

Method	Overall median accuracy (pixels (%))		Median validation accuracy of each class (pixels (%))		Qualified runs	Spectral processing
	Calibration	Validation	HLTY	HLB		
NBC1	48 (80.0)	35 (63.6)	4 (26.7)	31 (77.5)	16	Norm
KNN1	46 (76.7)	32 (58.2)	5 (33.3)	27 (67.5)	100	None
SVM1	48 (80.0)	35 (63.6)	5 (33.3)	29 (72.5)	100	1-Diff
LDB	44 (73.3)	37 (67.3)	5 (33.3)	32 (80.0)	75	1-Diff
NBC2	39 (65.0)	36 (65.5)	6 (40.0)	29 (72.5)	5	1-Diff
KNN2	41 (68.3)	33 (60.0)	6 (40.0)	27 (67.5)	27	1-Diff
SVM2	41 (68.3)	34 (61.8)	7 (46.7)	27 (67.5)	31	1-Diff

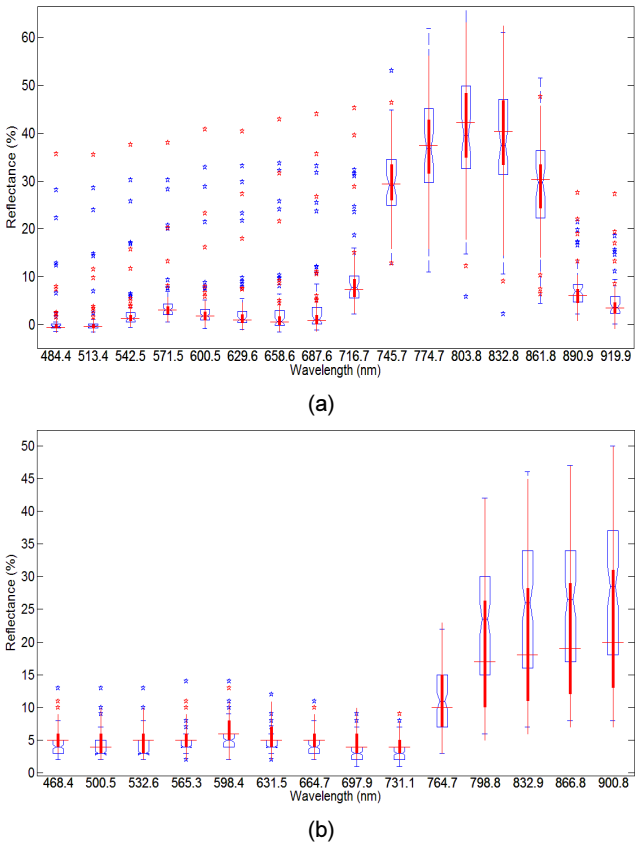

Figure 5. Box plot of the spectrum of the healthy (blue) and HLB infected (red) pixels for SG and CREC images: (a) SG Image and (b) CREC Image.

of disqualified runs was calculated as '100 (total runs) - qualified runs'.

It can also be seen that the number of qualified runs was usually low except for SVM1 and KNN1. While the overall accuracy was not too poor, the median HLTY accuracy was lower than 50% in all cases during validation. Of the many factors causing it was imaging late in the afternoon when the sun was at an angle rather than overhead. Thus each pixel was a result of mixing of signals of not only the healthy and infected canopies but also the background and the shadows formed by the lower angle of the sun. Other factors included the low band selectivity in case of FFSA based methods, relatively large pixel size, and fewer HLTY samples. Therefore, each misclassified pixel was a bigger setback to the class accuracy. The median false positive rate for the SG data (data not shown) was quite high with all methods exceeding 50%. The HLTY and HLB accuracy have been listed for the validation stage. A good result would have similar performance for HLB and healthy classes. Poor performance for one of the classes implied that spectra of the healthy and infected pixels were quite similar. The box plot in Figure 5 indicates that they indeed were quite similar as evidenced by the narrow gap between the mean spectra of healthy and infected. Plots for HLTY are in blue and HLB in red in Figure 5. The rectangular boxes (narrow and filled; and wider and empty) represent data within 25 and 75 percentile. The notch for the empty box and the line for the filled box near their center represent the median.

Along with the thin lines extending from the central box (called whiskers), the box plots represent approximately 99.3% of the available data in a band. The remaining 0.7% is outliers which have been represented individually by stars. Many outliers can be observed in the SG grove image in the 500-700 nm range and again in the 900 nm range; both HLB and HLTY sets contained a lot of outlier pixels.

The results for the CREC image of 2011 in Table 4 appear to be a little more balanced than the SG classification results owing to slightly better separation between the classes. This implies that the accuracy of classification of healthy pixels was higher and both sets were contributing more equally to the final classification accuracy. This is a requirement of good classification

Table 4. Accuracy of all the algorithms for the CREC grove

Method	Overall median accuracy (pixels (%))		Median validation accuracy of each class (pixels (%))		Qualified runs	Spectral processing
	Calibration	Validation	HLTY	HLB		
NBC1	62 (77.5)	55 (66.3)	16 (53.3)	38 (71.7)	100	Norm
KNN1	63 (78.8)	53 (63.9)	15 (50.0)	37 (69.8)	100	1-Diff
SVM1	65 (81.3)	59 (71.1)	20 (66.7)	40 (75.5)	100	1-Diff
LDB	62 (77.5)	59 (71.1)	18 (60.0)	41 (77.4)	100	Norm
NBC2	52 (65.0)	53 (63.9)	19 (63.3)	35 (66.0)	82	None
KNN2	53 (66.3)	53 (63.9)	18 (60.0)	36 (67.9)	67	1-Diff
SVM2	58 (72.5)	60 (72.3)	21 (70.0)	38 (71.7)	90	None

because it means that the classifier is able to distinguish between the two classes better.

The number of disqualified results was observed to be fewer on the whole as well – it was zero for all the FFSA based methods and in general less than a half of the disqualified runs for the 2010 image. Almost all the results for a particular case (NBC2) for the SG grove and about 70% in general had to be discarded. But less than a half of that number (30%) had to be discarded for the CREC image.

Discussion

The first aim of the study, namely band selection, was successfully implemented using FFSA. The number of bands were reduced from 128 (SG image) or 98 (CREC) to about five or fewer depending on the classification method in consideration. Similar levels of reduction in the number of bands were achieved for both images. It was also observed that classification was better in general when band selection was used along with classification.

For both images, it was observed that learning accuracy was better when fewer bands were used than when all the bands were used. Most techniques using all bands failed to train well enough to produce 50% individual class accuracy despite an overall accuracy of about 70%. Thus, feeding all the bands to the classifier may be detrimental to classification because most of the data is redundant and there is no mechanism to reject this useless information.

In those runs where the "all band" methods produced acceptable results, the total accuracy was comparable to FFSA based methods. Also comparison of calibration and validation accuracies shows that for techniques without FFSA, the difference in results between calibration and validation was smaller. Difference in accuracies of almost 20% was observed between calibration and validation for FFSA techniques. But it was less than 10% for non-FFSA techniques. Training was also much faster for the non-FFSA methods. But the advantages of using fewer bands and better learning (minimum 50% for each class individually) heavily outweighed the speed benefits.

The methods tested had different levels of computational complexity starting from the simple KNN technique to the probabilistic approach of NBC, and the more complex SVM and LDB. The more complex ones required more time to compute the results. While the different methods did not have drastically different results, considering the complexity and time taken SVM seemed to have a good balance of accuracy and computation time giving more priority to accuracy. NBC and KNN were much faster but slightly less accurate. LDB was slower but a little more consistent with its results, i.e., the validation accuracy and calibration accuracies were more comparable. The poorer performance of KNN could be attributed to poorer band selection - KNN results were based on an average of just 1 band, while the other methods chose on average 2 or more. LDB tended to have a slightly higher false positive rate compared to SVM1 but lower than KNN1 in general.

Comparing the accuracies of the different methods, most had a median accuracy of 60-70%. This is comparable to - and in some instances better than - the results of Kumar et al. (2012) and Li et al. (2012), who used SAM, spectral information divergence (SID), spectral feature fitting (SFF), MTMF, etc. on the same or similar datasets. Thus, it may not always be necessary to utilize standard hyperspectral classification methods. Commonly used, simpler methods can work equally well. Among the methods tested, SVM – in combination with FFSA – seems to be the best contender.

Conclusions

This study completely supports the premise that band selection improves results when compared to using all the bands. Forward feature selection algorithm performs this task efficiently; it can improve the performance of even simple techniques such as KNN and bring it on par with techniques designed for hyperspectral information such as SAM, SID, MTMF, etc. Among the methods tested, SVM seemed to be the best compromise between complexity or execution time and accuracy; SVM was a good method for use both with FFSA and without. LDB followed SVM in accuracy for the FFSA based method and finally NBC and KNN.

It can also be inferred that pre-processing techniques like normalization and spectral difference play a useful role in classifying these similar datasets. And until better spatial resolution can be achieved, classification errors have to be reduced through data pre-processing (normalization, spectra difference, etc.) or combining different methods to exploit different advantages (e.g., KNN and FFSA or

SVM and FFSA, etc.). Results for field measurements in Li et al. (2012) compared against the airborne imagery supports the need for better resolution images.

Conflict of Interest

The authors have no conflicting financial or other interests.

Acknowledgement

This project was funded by the Citrus Research and Development Foundation, Inc. The authors would like to thank Dr. Han Li, Dr. Ce Yang, Dr. Xiuhua Li, Ms. Sherrie Buchanan and Mr. Sudhir Vyasaraja at the University of Florida for their assistance in the study.

References

Albritton, M. 2012. Sections (TRS) positive for Huanglongbing (HLB, Citrus Greening) in Florida. Available at: www.freshfromflorida.com/pi/chrp/greening/StatewidePositiveHLBSections.pdf.

Bajwa, S. G., P. Bajcsy, P. Groves and L. F. Tian. 2004. Hyperspectral image data mining for band selection in agricultural applications. Transactions of the ASAE 47(3):895-907.

Boardman, J. W. and F. A. Kruse. 1994. Automated spectral analysis: A geologic example using AVIRIS data, north Grapevine Mountains, Nevada. In: *Proceedings of the Thematic Conference on Geologic Remote Sensing* 10(1):407-418.

Brlansky, R. H., K. R. Chung and M. E. Rogers. 2005. 2006 Florida citrus pest management guide: Huanglongbing (citrus greening). UF/IFAS Extension.

Candade, N. and B. Dixon. 2004. Multispectral classification of Landsat images: A comparison of support vector machine and neural network classifiers. ASPRS Annual Conference Proceedings, Denver, Colorado.

Cestnik, B. 1990. Estimating probabilities: a crucial task in machine learning. In: *Proceedings of the European Conference on Artificial Intelligence*, pp. 147-149, Stockholm, Sweden,.

Cover, T. and P. Hart. 1967. Nearest neighbour pattern classification. IEEE Transactions on Information Theory 13(1):21-27.

Demir, B. and S. Erturk. 2007. Hyperspectral image classification using relevance vector machines. IEEE Transactions on Geoscience and Remote Sensing Letters, 4(4):586-590.

Garnier, M., S. Jagoueix-Eveillard, P. R. Cornje, H. F. Le Roux and J. M. Bove. 2000. Genomic characterization of a Liberibacter present in an ornamental rutaceous tree, Calodendrum capense, in the Western Cape province of South Africa. Proposal of 'Candidatus Liberibacter africanus subsp. capensis'. International Journal of Systematic and Evolution Microbiolog 50:2119-2125.

Huang, W., D. W. Lamb, Z. Niu, Y. Zhang, L. Liu and J. Wang. 2007. Identification of yellow rust in wheat using in-situ spectral reflectance measurements and airborne hyperspectral imaging. Precision Agriculture 8(4-5): 187-197.

Kong, W., C. Zhang, F. Liu, P. Nie and Y. He. 2013. Rice seed cultivar identification using near-infrared hyperspectral imaging and multivariate data analysis. Sensors 13: 8916-8927.

Kumar, A., W. S. Lee, R. Ehsani, L. G. Albrigo, C. Yang and R. L. Mangan. 2012. Citrus greening disease detection using aerial hyperspectral and multispectral imaging techniques. Journal of Applied Remote Sensing 6, 063542.

Kumar, S., J. Ghosh and M. M. Crawford. 2001. Best-bases feature extraction algorithms for classification of hyperspectral data. IEEE Trans. Geosci. Remote Sens 39(7): 1368-1379.

Kuo, B., J. Yang, T. Sheu and S. Yang. 2008. Kernel-based KNN and Gaussian classifiers for hyperspectral image classification. Geoscience and Remote Sensing Symposium, IEEE International, II-1006-II-1008.

Li, X., W. S. Lee, M. Li, R. Ehsani, A. R. Mishra and C. Yang. 2012. Spectral difference analysis and airborne imaging classification for citrus greening infected trees. Computers and Electronics in Agriculture 83:32-46.

Matsuo, K., M. Iwate, K. Nishiwaki, S. Zhang and M. Yashiro. 2006. Development of experimental setup for distinction of disease plant. ASABE Paper No. 063016, St. Joseph, Mich.: ASABE.

Melgani, F. and L. Bruzzone. 2004. Classification of hyperspectral remote-sensing images with support vector machines. IEEE Transactions on Geoscience and Remote Sensing 42(8):1778-1790.

Sankaran, S., A. Mishra, R. Ehsani and C. Davis. 2010. A review of advanced techniques for detecting plant diseases. Computers and Electronics in Agriculture 72(1):1-13.

Shafri, H. Z. M. and N. Hamdan. 2009. Hyperspectral imagery for mapping disease infection in oil palm plantation using vegetation indices and red edge techniques. American Journal of Applied Sciences 6(6):1031-1035.

Qin, J., T. F. Burks, M. A. Ritenour and W. G. Bonn. 2009. Detection of citrus canker using hyperspectral reflectance imaging with spectral information divergence. Journal of Food Engineering 93:183-191.

Qin, Z. and M. Zhang. 2005. Detection of rice sheath blight for in-season disease management using multispectral remote sensing. International Journal of Applied Earth Observation and Geoinformation 115-128.

Rouse, J. W., R. H. Haas, J. A. Schell and D. W. Deering. 1973. Monitoring vegetation systems in the Great Plains with ERTS. Third ERTS Symposium, NASA SP-351 I: 309-317.

USDA. 2012. 2010-2011 Citrus summary. Available at: www.nass.usda.gov/Statistics_by_State/Florida/Publications/Citrus/cspre/cit92211.pdf.

Whitney, A. W. 1971. A direct method of nonparametric measurement selection. IEEE Transactions on Computers 20: 1100-1103.

Williams, P. J., P. Geladi, T. J. Britz and M. Manley. 2012. Near-infrared (NIR) hyperspectral imaging and multivariate image analysis to study growth characteristics and differences between species and strains of members of the genus Fusarium. Analytical and Bioanalytical Chemistry 404: 1759-1769.

Yang, C. 2010. An airborne four-camera imaging system for agricultural applications. ASABE Paper No. 1008855, St. Joseph, Mich.: ASABE.

Yang, C. M. 2010. Assessment of the severity of bacterial leaf blight in rice using canopy hyperspectral reflectance. Precision Agriculture 11:61-81.

Yang, C., J. H. Everitt, M. R. Davis and C. Mao. 2003. A CCD camera-based hyperspectral imaging system for stationary and airborne applications. Geocarto International 18(2):71-80.